

## The dark-matter axion mass

---

**Vincent B. Klaer, Guy D. Moore**

*Institut für Kernphysik, Technische Universität Darmstadt  
Schlossgartenstraße 2, D-64289 Darmstadt, Germany*

*E-mail:*

[vklaer@theorie.i kp.physik.tu-darmstadt.de](mailto:vklaer@theorie.i kp.physik.tu-darmstadt.de), [guy.moore@physik.tu-darmstadt.de](mailto:guy.moore@physik.tu-darmstadt.de)

**ABSTRACT:** We evaluate the efficiency of axion production from spatially random initial conditions in the axion field, so a network of axionic strings is present. For the first time, we perform numerical simulations which fully account for the large short-distance contributions to the axionic string tension, and the resulting dense network of high-tension axionic strings. We find nevertheless that the total axion production is somewhat *less* efficient than in the angle-averaged misalignment case. Combining our results with a recent determination of the hot QCD topological susceptibility [1], we find that if the axion makes up all of the dark matter, then the axion mass is  $m_a = 26.2 \pm 3.4 \mu\text{eV}$ .

**KEYWORDS:** axions, dark matter, cosmic strings, global strings

---

## Contents

<b>1</b>	<b>Introduction</b>	<b>1</b>
<b>2</b>	<b>Methodology</b>	<b>3</b>
<b>3</b>	<b>Numerical results</b>	<b>4</b>
3.1	Lattice spacing	4
3.2	Initial network density	6
3.3	Thin-core limit	7
3.4	String tension and temperature-dependent susceptibility	9
<b>4</b>	<b>Discussion</b>	<b>12</b>
<b>A</b>	<b>Algorithmic details</b>	<b>14</b>
<b>B</b>	<b>Other numerical tests</b>	<b>15</b>

---

## 1 Introduction

The QCD axion [2, 3] is a hypothetical particle, predicted in models which solve the QCD theta problem [4–6] via the Peccei-Quinn mechanism [7, 8]. In the simplest models [9, 10] it is the angular mode of a complex scalar,  $\sqrt{2}\varphi = fe^{i\theta_a}$  or  $\theta_a = \text{Arg}\varphi$ , which would be the Goldstone boson of a spontaneously broken U(1) symmetry, except that the symmetry is also anomalous (explicitly broken by QCD). Therefore QCD effects induce a small, temperature-dependent “tilt” in the potential, and therefore make the angular fluctuations massive, so the axion mass is  $m_a \neq 0$ . The axion is a dark matter candidate [11–13] because early Universe dynamics generically generate large coherent oscillations in the axion field – essentially a Bose-Einstein condensate of axions at or near rest – which act as a pressureless fluid on scales longer than a few meters.

In this paper we will predict the axion’s mass, given the following hypotheses:

1. the axion exists;
2. PQ symmetry is restored either during or at some point after inflation, so that the axion field starts out “random,” meaning that its value at points out of post-inflationary causal contact are uncorrelated [14, 15];
3. The cosmological epoch where axions are produced – roughly, temperatures around 1 GeV – follows standard FRW behavior with the expected standard-model matter content;

4. the axion makes up 100% of the dark matter, so its current energy density is set by measurements of  $\Omega_{\text{dm}} h^2$ ;  $\rho_{\text{dm}}/s = 0.39 \text{ eV}$  with  $s$  the entropy density [16].

These assumptions give rise to a rich dynamics, with a network of axionic cosmic strings [17] which collapses once the axion mass becomes large in units of the system age,  $m_a t \gg 1$ , through the action of axionic domain walls [18], leaving a final state with small-amplitude axionic fluctuations which evolve adiabatically thereafter. Under our assumptions, a mass prediction should be possible, because the model has one principal free parameter,<sup>1</sup> the axion “decay constant” (the vacuum expectation value breaking the U(1) symmetry)  $f_a$  (defined below in Eq. (2.1)). This parameter determines the axion mass, see Eq. (2.2). And given our other assumptions, it also sets the dark matter density. By computing the relation between  $f_a$  and the dark matter density, we should then be able to predict  $f_a$  and therefore  $m_a$ . Such a prediction is valuable because it informs experiment, and because if the axion is then discovered at this mass, it will clarify its role as the dark matter.

In the next section, we lay out our methodology for relating  $f_a$  to the axionic dark matter density. Section 3 presents our numerical results. We end with a discussion. A few technical issues and numerical tests are postponed to an appendix. But for the impatient reader, we present our main results here. While there have been numerous previous studies of this problem [21–30], ours is the first which includes the physics of the large tension associated with axionic strings. This large tension leads to a much higher density of strings which are more robust and survive longer than in previous simulations. However, this makes surprisingly little difference in the final axion number produced. Let us set as a baseline for axion production, the angle-averaged misalignment value of the axion density. This is the axion density value we would find if the axion field starts out uniform in space with value  $\theta_a$ , averaged over  $\theta_a \in [-\pi, \pi]$  (without the approximation, sometimes made, of replacing  $1 - \cos \theta_a \rightarrow \theta_a^2/2$  in the potential)<sup>2</sup>. At a given  $f_a$  value, we find the axion number density produced in the inhomogeneous case is actually *smaller* than the misalignment value, by a factor of about 0.78. Since  $\rho_{\text{dm}}$  increases with increasing  $f_a$ , this inefficiency must be compensated by a larger value of  $f_a$ , and hence a smaller value of  $m_a$ , than has generally been assumed; we find  $m_a \simeq 26.2 \pm 3.4 \mu\text{eV}$ . We postpone discussion of this result and its errors to the conclusions.

<sup>1</sup>There are two other relevant parameters. There is the number  $N_a$  of minima around the U(1) circle,  $\cos \text{Arg } \varphi \rightarrow \cos N_a \text{Arg } \varphi$ . But if  $N_a \neq 1$  then the model predicts stable domain walls which are a cosmological disaster [19, 20]. Also there is the mass of the radial excitation in the complex scalar field,  $m$ . This must be heavy, and we find below that the results are quite weakly dependent on its exact value.

<sup>2</sup>Specifically, we write the conformal-time axion mass squared as  $m_a^2 = t^{n+2}/t_*^{n+4}$  ( $t$ ,  $n$ , and  $t_*$  defined in the next section) and evolve  $\theta(t)$  according to  $d^2\theta/dt^2 + (2/t)d\theta/dt = -m_a^2 \sin \theta$  to a time  $t > 4t_*$ . The axion number density at time  $t$  is  $n_{\text{ax}} = (m\theta^2 + \dot{\theta}^2/m)/2$ . We average over starting values  $\theta \in [-\pi, \pi]$  and use the resulting  $n_{\text{ax}}$  average to normalize the result of a string simulation at the same  $t/t_*$  value.

## 2 Methodology

Our approach will be as follows. The Lagrangian for the axion field is<sup>3</sup>

$$-\mathcal{L} = g^{\mu\nu} \partial_\mu \varphi^* \partial_\nu \varphi + \frac{m^2}{8f_a^2} (2\varphi^* \varphi - f_a^2)^2 + \chi(T) (1 - \cos \theta_a). \quad (2.1)$$

The middle term is the symmetry breaking Lagrangian, and the last term is the “tilt” in the potential due to QCD effects. This tilt gives rise to an axion mass of

$$m_a^2(T) = \frac{\chi(T)}{f_a^2}, \quad m_a^2(T=0) = \frac{\chi(T=0)}{f_a^2}. \quad (2.2)$$

In a radiation dominated FRW universe, in comoving coordinates and conformal time, the metric is  $g_{\mu\nu} = t^2 \eta_{\mu\nu}$  and the temperature is  $T \propto t^{-1}$ , so

$$-\sqrt{g} \mathcal{L}_{\text{conf}} = t^2 \left( -\dot{\varphi}^* \dot{\varphi} + \nabla \varphi^* \cdot \nabla \varphi + t^2 \frac{m^2}{8f_a^2} (2\varphi^* \varphi - f_a^2)^2 + t^2 \chi(t) (1 - \cos \theta_a) \right). \quad (2.3)$$

Here  $\chi(T(t))$  is the topological susceptibility. Model calculations [31] and a recent lattice calculation [1] indicate that  $\chi(T)$  is approximately power law between 1.5 GeV and 400 MeV, which, we will see, is wider than the relevant temperature range we need. Therefore we will treat  $\chi(T)$  as a power law,  $\chi(T) \propto T^{-n}$ , so  $t^2 \chi(t) = f_a^2 t^{n+2}/t_*^{n+4}$ , with  $t_*$  the natural scale where the susceptibility begins to influence the dynamics;  $t_* m_{a,\text{conf}}(t_*) = 1$  where  $m_{a,\text{conf}} = \sqrt{t^2 \chi(t)}/f_a$  is the conformal-time axion mass. In terms of physical time,  $t_*$  is the moment when  $m_a H = 1$ . In the following we will suppress the subscript and write  $m_{a,\text{conf}} = m_a$ , except in the discussion. That is, masses and times will always be expressed in conformal units.

To initialize the network, we choose an independent random phase at every lattice site. We then evolve the fields for an initial time under strong damping ( $\ddot{\varphi} + 2\dot{\varphi}/t \rightarrow \ddot{\varphi} + k_{\text{max}} \dot{\varphi}/t$  for times  $t < t_{\text{start}}$ ) to prepare a string network relatively close to the scaling network density. The length and strength of damping is chosen such that the string network will roughly match on to the scaling network density; we will also study the dependence on the initial conditions below.

The model has two sorts of metastable defects, strings and domain walls. A string is identified as a linear structure where  $\theta_a$  changes by  $2\pi$  in circling the string. A domain wall is a surface on which  $\theta_a = \pi$ ; each string has one such domain wall ending on it. The domain walls only become distinct structures once  $m_a t \gg 1$ ; the surface tension of an isolated domain wall is  $\sigma = 8m_a f_a^2$ , which grows rapidly with time. Therefore the domain walls straighten out and pull the strings together, annihilating both networks and leaving small fluctuations in the  $\theta_a$  field. We evolve all fields until this dynamics is complete and there are no strings left. Then we count the axion abundance by extracting  $\theta_a$  and  $d\theta_a/dt$  from the simulation and applying the method of [29] to determine the axion content. This determines the total density of axions from all sources – we make no attempt to distinguish which axions arise from strings, from walls, or from misalignment, as we do not believe

---

<sup>3</sup>We use  $[-+++]$  metric convention, and standard complex-field normalization  $\varphi = (\varphi_r + i\varphi_i)/\sqrt{2}$ .

such a distinction can be made unambiguously. We express the axion number produced as a ratio to the angle-averaged misalignment value and we determine  $f_a$  such that the dark matter abundance is correct.<sup>4</sup>

The scale  $m$  for “radial” excitations in the  $\varphi$  field is may be as large as  $m \sim f_a \sim 10^{11}\text{GeV}$  and must be at least  $10^3\text{GeV}$  (see Subsection 3.4), while the relevant length scale is  $H$  at the QCD epoch (around 1 GeV temperature), which is of order  $10^{-18}\text{GeV}$ . We handle this huge scale hierarchy by observing that the only important physics it gives rise to is very thin, high-tension axionic cosmic strings. Specifically, the string tension should be  $T_{\text{str}} \simeq \kappa \pi f_a^2$  with  $\kappa \equiv \ln(m/H) \in [50, 70]$ . We address this physics via the technique we recently introduced [32]. Specifically, we add abelian-Higgs degrees of freedom which are massive away from string cores but which induce a large string tension. In the Appendix A we review the procedure and explain how we implement  $\chi(T)(1 - \cos \theta_a)$  into this method. The outcome is that the string tension is maintained by some extra, massive degrees of freedom, but the mass scale  $m$  for these degrees of freedom must be resolved by the lattice,  $ma \lesssim 1$  with  $a$  the lattice spacing. The correct physical limit involves this scale becoming heavy compared to the physics of IR fluctuations in the axion field. Since the correct physical picture arises when  $m$  is large, we will hold  $ma$  fixed, that is, we keep  $m$  fixed in lattice units, throughout a simulation. In our implementation, the extra degrees of freedom introduce one new parameter  $q_1$ , which determines the value added to  $\kappa$ ; most of our results are labeled  $(q_1, q_2) = (4, 3)$ , which means that  $\kappa$  has been increased by 50 through the added degrees of freedom [32].

### 3 Numerical results

In Appendix B we show that our results are in the large volume limit if we keep  $L/t_* \geq 5$ , and we show that the axion number does not evolve after the string network is gone and can be measured as soon as no string is left, without concern that it will evolve further. Therefore box size and axion number measurement do not contribute to our error budget. Here we will instead focus on those effects which still do.

#### 3.1 Lattice spacing

For axionic strings to evolve correctly, the string core must be resolved by our lattice spacing. We need to check that our lattice is fine enough, in the sense of  $ma$  the product of the heavy scale and the lattice spacing is sufficiently small. That said, numerical cost scales as  $(ma)^{-4}$  and required RAM scales as  $(ma)^{-3}$ , so we want the largest value which we can get away with. To test the  $(ma)$  dependence, we fix all other parameters in terms of  $m$ , and we consider axion production at various  $ma$  values in Figure 1. Because we have used an improved action, the result should naively converge in the small  $ma$  limit with corrections vanishing as  $(ma)^4$ , motivating the axis choice in the left-hand plot. However, the right-hand plot shows that the data fit better assuming  $(ma)^2$  dependence. Indeed the  $\chi^2$  for an  $(ma)^2$  fit is about 1, while for an  $(ma)^4$  fit,  $\chi^2 = 15$ . Therefore we will assume

---

<sup>4</sup>We implement the misalignment case in the same code by turning off the scalar gradient terms. We also implemented misalignment in a simple dedicated code as a cross-check.

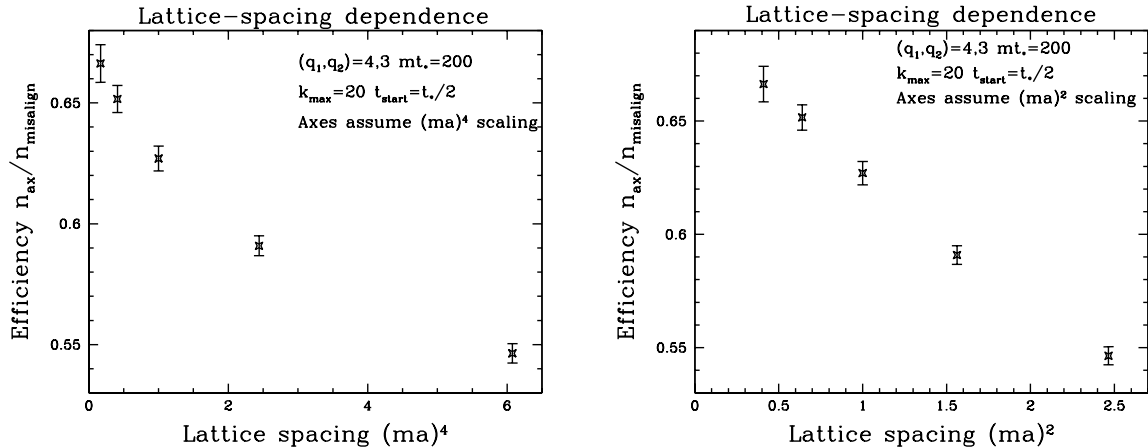


**Figure 1.** Dependence of the axion production rate on the lattice spacing  $a$ , expressed as a function of  $ma$  with all else held fixed in units of  $m$ .

that the errors are quadratic in spacing, despite our improved action. The fit indicates an upwards correction between  $(ma) = 1$  and the continuum limit  $(ma) = 0$  of  $10 \pm 1\%$ . In the rest of this study we will use  $ma = 1$  and correct the final results upwards by 10%.

It remains to explain why the axion production scales with  $(ma)^2$  despite our improved action, which should give  $(ma)^4$  convergence if fields are smooth. We believe this occurs because a small fraction of string has a velocity close to 1, and therefore a large Lorentz contraction factor. If the (energy-weighted) fraction of string with velocity-squared  $v^2 > v_0^2$  only vanishes linearly in the  $v_0^2 \rightarrow 1$  limit, then the fraction of string with  $\gamma^{-2} < \epsilon$  would then scale linearly in  $\epsilon$ . Such scaling is consistent with our measured string velocity distribution. It also makes sense from the string equations of motion. In flat space, with  $\chi = 0$ , and in the Nambu-Goto limit, labeling the string location as  $x_i(\sigma, t)$  with  $\sigma$  an affine parameter along the string, one can make a gauge choice such that  $\dot{x}_i x'_i = 0$  and such that  $\sqrt{x'_i x'_i / (1 - \dot{x}_j \dot{x}_j)} = 1$ . The equation of motion is then

$$\ddot{x}_i = x''_i \quad (3.1)$$

which is solved by [33–35]

$$x'_i = \frac{\alpha_i(\sigma+t) + \beta_i(\sigma-t)}{2}, \quad (3.2)$$

$$\dot{x}_i = \frac{\alpha_i(\sigma+t) - \beta_i(\sigma-t)}{2}, \quad (3.3)$$

$$\alpha_i(r)\alpha_i(r) = 1 = \beta_i(r)\beta_i(r) \quad \forall r. \quad (3.4)$$

Here  $\alpha, \beta$  are backwards and forwards propagating waves which take values on the unit sphere. Even in curved space we may satisfy the gauge choice instantaneously. The relevant question for the distribution of string velocities is the distribution of angles between  $\alpha$  and  $\beta$ , since  $v^2 = \dot{x}^2 = (1 - \alpha \cdot \beta)/2$ . The *measure* of  $\alpha \cdot \beta$  values is uniform in  $[-1, 1]$  because  $\alpha, \beta$  take values on the unit sphere. While we do not expect the distribution of  $\alpha \cdot \beta$  values to be uniform in  $[-1, 1]$ , neither do we have a reason why it should avoid  $\alpha \cdot \beta = -1$ , so the

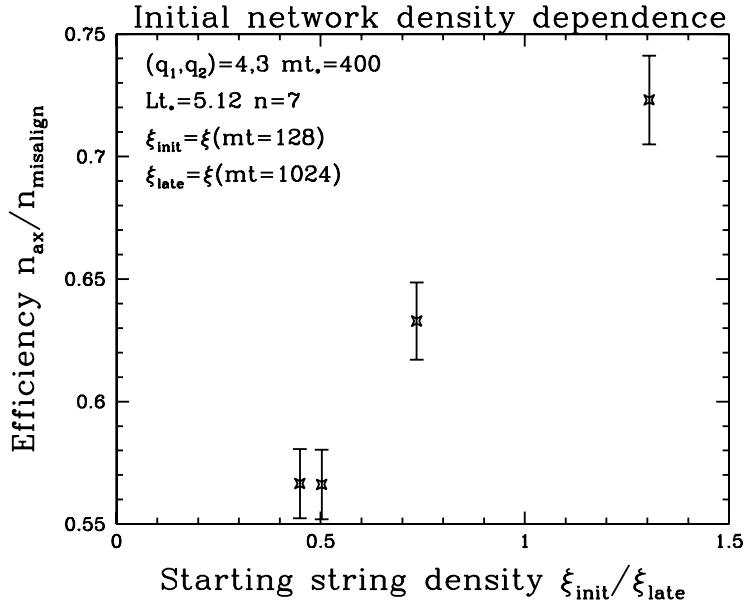


**Figure 2.** Dependence of the final axion density on the initial string network density. We measure the starting network density as the ratio between the scaled density  $\xi$  at time  $mt = 128$  ( $t/t_* = 0.32$ ) and the scaled density at time  $mt = 1024$ , shortly before the walls start to influence the network evolution ( $t/t_* = 2.56$ ).

probability distribution should not vanish at  $\alpha \cdot \beta = -1$ , and therefore the fraction of string with  $\gamma^{-2} < \epsilon$  should indeed vanish linearly in small  $\epsilon$ . Consider  $\epsilon = (ma)^2$ , corresponding to a gamma-factor of  $\gamma > 1/ma$  and therefore a Lorentz contracted string thickness<sup>5</sup> of  $\gamma^{-1}(1/m) < a$ . Our hypothesis for string velocities then states that an  $\mathcal{O}((ma)^2)$  fraction of string should be Lorentz contracted to a thickness of less than 1 lattice spacing. Such string is mistreated regardless of how improved our update algorithm is. Therefore, even if typical string is treated correctly with  $\mathcal{O}((ma)^4)$  errors, the fraction which is mistreated is of order  $(ma)^2$ . This allows  $(ma)^2$  scaling corrections, regardless of the level of lattice action improvement.

### 3.2 Initial network density

We want the axion production from a string network which is initially in the scaling regime. But this cannot be exactly achieved; initial conditions will typically produce a network which is either denser or less dense than scaling. The network evolves towards scaling, and if  $mt_*$  is large enough then initial conditions should have little effect. But it would still be good to check how sensitive the final axion number is to the starting conditions.

We address this in Figure 2. We introduce the scaled network density

$$\xi = \frac{t^2 \int_{\text{all string}} \gamma dl}{4V_{\text{space}}}, \quad (3.5)$$

<sup>5</sup>In this parametric argument we are neglecting order-1 factors which make the string somewhat thicker than  $1/m$  and mean that, for  $ma = 1$ , most string is actually properly treated.

with  $\gamma$  the local gamma-factor of the string so that the integral represents the total invariant length of string (length scaled by a  $\gamma$  factor to account for the energy content), and with  $V_{\text{space}}$  the volume of the simulation. This combination should approach a fixed “scaling” value as  $t$  increases (for  $\chi(T) = 0$ , that is, in the absence of potential tilt). We measure  $\xi$  once early in an evolution and again later in the evolution, just before the walls start to influence the string network evolution. We perform several evolutions with initial conditions with more or less damping, leading to denser or rarer initial networks. The ratio of the starting to final  $\xi$ ,  $\xi_{\text{init}}/\xi_{\text{late}}$ , then indicates whether the network started too thin or too dense, and therefore from which side it is approaching the scaling solution. We find a roughly linear correlation between this starting density and axion production, with more axions arising from denser starting networks. However the dependence is quite weak. Based on the figure, we will try to use initial conditions with this  $\xi$  ratio close to 1, and we will assign a 5% systematic error based on incomplete network scaling.

### 3.3 Thin-core limit

Next we must consider the effects of finite  $mt_*$ , meaning that the strings are of finite thickness. This is clearly an artifact because in the physical case there is a hierarchy of many orders of magnitude between string thickness and axion mass. We have incorporated the logarithmic sensitivity to this hierarchy by implementing auxiliary fields to give rise to the resulting high string tension. But there can still be effects suppressed by powers of  $1/(mt_*)$ , probably starting at first order. In particular, strings may lose energy via the radiation of unphysical massive modes. We only expect such radiation from short length-scale structures on the strings, which should generally get smoothed out by axion emission so long as  $mt_* \gg \kappa$  and  $m_a/m \ll 1$ . However, because  $m_a$  grows as a large power of conformal time,  $m_a \propto t^{1+\frac{n}{2}}$ , the latter condition may not be maintained, given the persistence of high-tension strings. And if the axion mass  $m_a$  comes of order the heavy-mode mass  $m$  then one might expect that axion production is lost to heavy-mode production, and the simulation could result in an *underestimate* of axion production.<sup>6</sup>

We can “fix” this problem by artificially capping the value of  $m_a$ , so that rather than growing with time at all times,  $t^2\chi(t)$  grows up to some value and then becomes constant. But this replaces one unphysical behavior with another, and it will introduce new artifacts. The axionic wall tension is proportional to  $m_a$ . These walls cause the network to collapse, and limiting their tension artificially extends the life of the network. We show this effect in Figure 3. The figure shows how the total length of strings, rescaled as in Eq. (3.5), and a similar rescaled wall area (without  $\gamma$  factor or the conventional factor of 4),

$$\xi_{\text{wall}} \equiv \frac{t \int_{\text{all wall}} d^2\Sigma}{V_{\text{space}}}, \quad (3.6)$$

evolve with time under the influence of various choices for a maximal  $m_a/m$  value. We see that the wall area starts to decline as the wall surface tension turns on around  $t = 1.6t_*$ ,

---

<sup>6</sup>In previous work [29] we showed that, for a theory of a pure scalar field, the axionic domain walls spontaneously decompose as soon as  $(m_a/m)^2 > 1/39$ . The added degrees of freedom in our string cores prevent this physics from occurring; the domain walls remain strongly metastable up to and past  $m_a/m = 1$ .

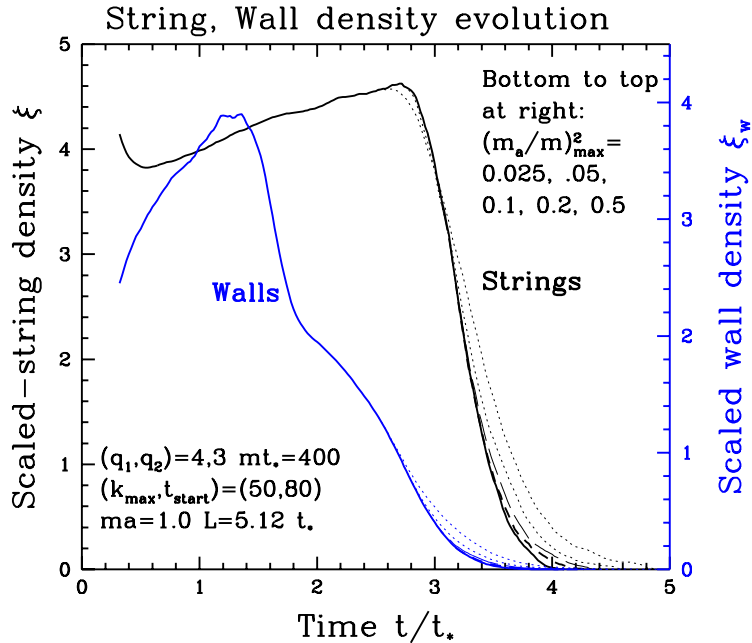


**Figure 3.** Density of walls and of strings as a function of  $t/t_*$  when the axion mass is artificially limited with 5 different limits.

and later around  $t = 2.8t_*$  the surface tension becomes large enough to influence the string network evolution, drawing together the strings and collapsing the network by  $t = 4t_*$ . However, artificially limiting the axion mass slows down the collapse of the network; for the smallest value we considered, the last bits of string survive almost to  $t = 5t_*$ .

We also expect that the network with a maximal  $m_a/m$  value will produce more axions than without such a cutoff.<sup>7</sup> The reason is that, as  $m_a$  increases, the energy stored in the string network becomes less and less useful for producing axions. While increasing  $m_a$  increases the energy in axion fluctuations and in domain walls in proportion to  $m_a$ , it does not change the energy in strings. Therefore, as  $m_a$  increases, the capacity for strings to make axions is diluted; since making an axion costs energy  $m_a$ , an energy  $E$  can only produce  $E/m_a$  axions. Limiting  $m_a$  turns off this dilution, allowing the string energy to produce more axions, and could therefore result in *overproduction* of axions.

The issue should disappear if we can reach a large enough value of  $mt_*$ . But it is useful to consider different cutoff values for  $m_a/m$  and take the large  $mt_*$  limit for each. If the continuum limits are the same, then it lends credence to the belief that we have achieved the continuum limit. According to Figure 4, The difference between different cutoff choices falls below 10% starting around  $mt_* = 300$  (third-from-leftmost points). On the two still-finer lattices, the choices  $(m_a/m)_{\max}^2 = 0.5$  and  $(m_a/m)_{\max}^2 = 0.2$  agree to within 3%. So these values can be close to the continuum limit. Note that the last point in the figure,

<sup>7</sup>Something special happens if we choose a maximum value for  $m_a$  which is very close to  $m/2$ . In this case, there is a resonant nonlinear mode-coupling process which converts mass  $m/2$  axions into mass- $m$  excitations, leading to a reduction in the axion production for values of  $(m_a/m)_{\max}$  very close to 0.5. This effect is clearly an artifact, so we avoid this special value.

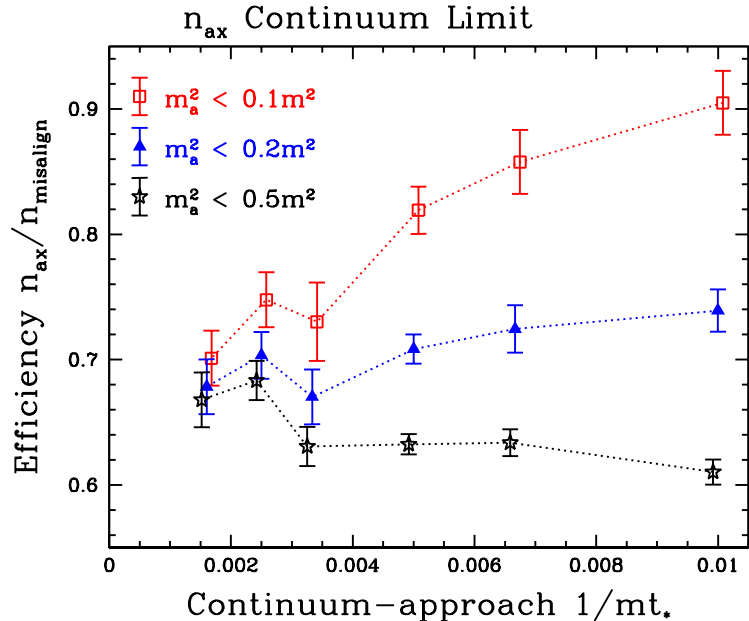


**Figure 4.** Axion production as a function of the continuum limit  $1/mt_* \rightarrow 0$  at three values of the artificial limiting value for the axion mass  $(m_a/m)_{\max}$ .

with  $mt_* = 625$ , was achieved by loosening  $ma$  from  $ma = 1.0$  to  $ma = 1.25$  and using the result of Figure 1 to extrapolate it to the same value as the other points; it is also at a slightly smaller physical volume,  $Lt_* = 4.1$  rather than 5.1.

The error bars shown in the figure are statistical only. However the statistical errors for points with the same  $mt_*$  value but different  $(m_a/m)_{\max}^2$  values are strongly correlated, since they are calculated from simulations which are identical up to the point when  $m_a$  reaches the smaller upper-bound value. Therefore the determination of the difference between different  $(m_a/m)_{\max}^2$  choices has smaller errors. In particular this difference is *not* linear in  $1/mt_*$ , but drops to a small value at a sufficient  $m_{a,\max}t_*$  value. That complicates the continuum limit. Here we will perform a linear extrapolation of the three smallest  $1/mt_*$  data points, each for  $(m_a/m)_{\max}^2 = 0.2$  and 0.5. We find 0.696(46) and 0.729(41) respectively. The fact that these answers are not the same indicates that our lattices are not yet abundantly fine. We assign a 10% error bar for the continuum-extrapolated value, to include these systematic issues, adopting  $n_{ax}/n_{misalign} = 0.71(7)$ . This is for  $n = 7$ ,  $\kappa = 50$  from extra degrees of freedom, and before performing the small  $ma$  extrapolation.

### 3.4 String tension and temperature-dependent susceptibility

Having discussed numerical artifacts, we now turn to actual physical parameters which are relevant but not completely known: the string tension  $\kappa$  and the strength of the temperature dependence  $n$  in  $\chi(T) \propto T^{-n}$ .

The slope  $n$  is calculable in lattice QCD. Recently Borsanyi *et al* have presented [1] results up to and beyond the relevant temperature range. Using their results at 600 and 1200 MeV, we estimate  $n = 7.6 \pm 0.5$ . Most groups find results which agree with Bor-

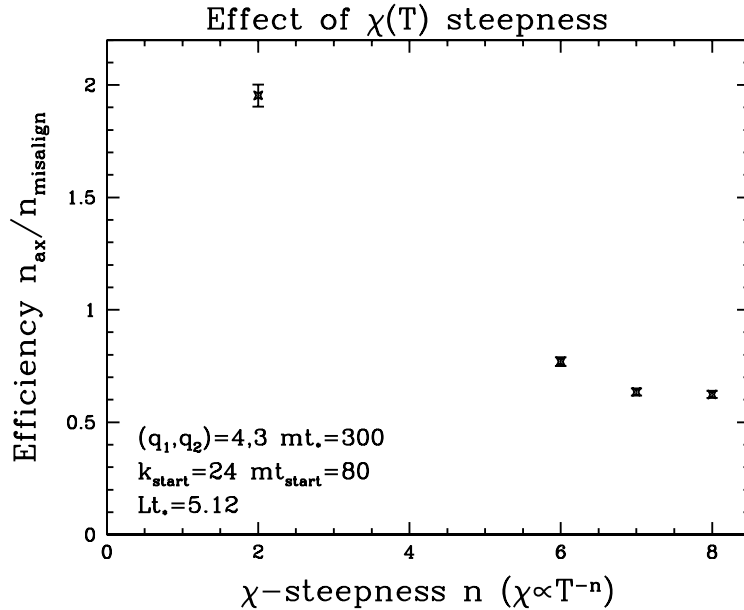


**Figure 5.** Dependence of the relative axion production efficiency on the parameter  $n$ , controlling how quickly  $m_a$  rises with  $t$ . For small  $n$  (gradually rising  $m_a$ ) the network produces more axions than in misalignment; for large  $n$  it produces fewer.

sanyi *et al* at lower temperatures [36–41], although no group has reproduced these higher temperatures and even below 600 MeV there are some results which appear discrepant [42, 43]. Therefore we will explore other  $n$  values but consider values near  $n = 7.5$  to be likely correct. We also feel that we gain some physical insight by considering different  $n$  values, especially much smaller values. We do this in Figure 5. The figure shows that small  $n$  values lead to more axions than in the misalignment mechanism, while large  $n$  values lead to less. But between  $n = 7$  and  $n = 8$  the dependence is not very strong. Therefore our choice to use  $n = 7$  elsewhere, which we made mostly for simplicity, does not appear to be very critical.

We interpret the results of Figure 5 as follows. The larger the  $n$ -value, the more rapidly the axion mass  $m_a$  turns on, and therefore the heavier the axion is when the string network breaks up and loses its energy. That means that for small  $n$ , the network can still produce relatively many of the relatively-light axions, but for large  $n$  the axions quickly become heavy and the string energy cannot produce a large number of them. This is consistent with what we saw when  $(m_a/m)_{\text{max}}^2$  was small. Indeed, the results at  $n = 2$  had  $(m_a/m)^2 = 0.07$  at the time the string network had completely disappeared, so walls broke up and axion production occurred when axions were still relatively light.

Finally we consider the  $\kappa$  value. Above we define  $\kappa$  as  $\kappa = \ln(m/H)$ . For us  $H = 1/t$  the inverse system age. Therefore the contribution from axionic modes to  $\kappa$  is  $\ln(mt)$ , which we approximate to its value at  $t = 3t_*$  since this is when the string network is breaking up. In addition there is a contribution from the extra massive degrees of freedom we have

added, so our simulations have

$$\kappa = \ln(3mt_*) + 2(q_1^2 + q_2^2), \quad (3.7)$$

where the charges  $(q_1, q_2)$  are explained in Appendix A.

We do not know what the physical value of  $\kappa$  should be, because we don't know the model-dependent microscopic origin of the axion field. In the single complex-field case [9, 10] we don't know the radial mass  $m$ ; if the axion is a composite or arises from more complicated physics [44], we do not know the compositeness scale and whether there is an extra contribution to the string tension from the microscopic physics giving rise to the axion field. We can reasonably guess that  $m < f_a \simeq 2 \times 10^{11}$  GeV. Also the requirement that the radial excitations decay by the time the Universe reaches a temperature of 1 GeV, along with an estimate for their decay rate [45],  $\Gamma_m \sim \frac{\alpha_s^2 m^3}{64\pi^3 f_a^2}$ , sets very roughly  $m > 10^3$  GeV. These limits correspond to approximately  $\kappa \in [48, 67]$ . For  $mt_* = 300$  and  $q_1 = 4$  the  $\kappa$  value in the simulation is  $50 + \ln(900) = 57$ , which is in this range. By considering other values of  $(q_1, q_2)$ , we achieve  $\kappa$  values larger and smaller than the physically interesting range.

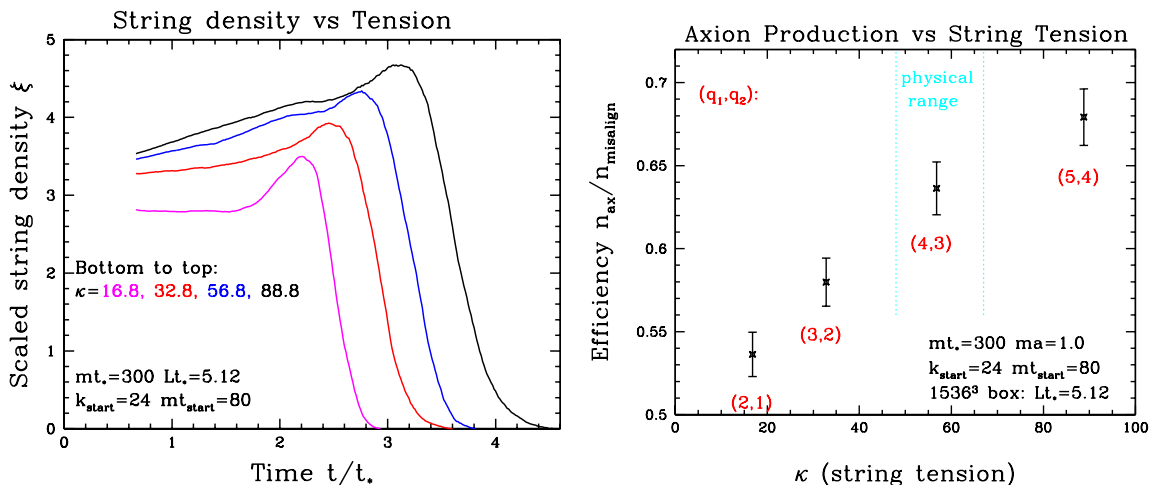


**Figure 6.** Left: string density as a function of time for different  $\kappa$  values. The higher the string tension, the longer the strings persist. Right: axion production efficiency as a function of  $\kappa$ .

We show results for the axion production as a function of  $\kappa$  in Figure 6. The figure shows that higher tension strings give a significantly denser string network, with strings which break up later, but nevertheless produces only mildly more axions (note the false zero for the y-axis in the right plot). Therefore our ignorance of the physical value of  $m$ ,  $\kappa$  is not very significant in bracketing the physical value of the axion. A simple linear fit to the left frame in Figure 6, and the range we quoted above for  $\kappa$ , gives a systematic error of  $\pm 3\%$  due to the unknown value of  $\kappa$ .

Note that the chosen initial conditions for both our  $n$  dependence and our  $\kappa$  dependence studies produced somewhat underdense networks. One can see in the left frame of Figure 6 that the underdensity is worse for the highest tensions, so the true  $\kappa$  dependence is

somewhat *underestimated*. Also note that the larger  $\kappa$  values are farther from the large  $mt_*$  limit, leading to a slight *overestimate* in the produced axions due to  $(m_a/m)_{\max}^2$  effects.

## 4 Discussion

If we take the temperature dependence of the topological susceptibility to scale as  $\chi(T) \propto T^{-n}$  with  $n = 7.6$  in the relevant temperature range [1], and assume that axionic string cores arise at a mass scale  $m \sim 10^7$  GeV so the extra string tension is  $\kappa = 58 \pm 10$ , then our results indicate an axion production efficiency which is 0.78(12) times as efficient as in the angle-averaged misalignment mechanism. The indicated error is dominated by the extrapolation to the large  $mt_*$  limit, with the uncertainty due to  $\kappa$  added linearly (not in quadrature).

Now we use this result to calculate the axion mass. There has been relatively little entropy production since the Universe was 1 GeV in temperature, so the ratio of axion number-density to entropy density is approximately the same at the end of the axion-production epoch as it is now. We can express our results by saying that the axion number density, determined at  $t = 4t_*$  or  $T = T_*/4$  and then back-extrapolated to the temperature  $T_*$  where  $m(T_*)H(T_*) = 1$ , was

$$\text{back-extrapolated } n_{\text{ax}}(T = T_*) \simeq KH(T_*)f_a^2, \quad (4.1)$$

where a numerical evaluation finds that the angle-averaged misalignment value for  $K$  is  $K = 16.61$ , and our result is  $K = 13.0 \pm 2.0$ . By dividing this by the entropy density at that temperature,  $s = 2g_*\pi^2T_*^3/45$ , we get the modern axion-number to entropy ratio, which can be multiplied by the vacuum axion mass  $m_a = \sqrt{\chi(T=0)}/f_a$  to give the modern dark matter density to entropy density ratio. We combine this with the Planck result [16],

$$\begin{aligned} \frac{n_b}{s} &\simeq 8.59 \times 10^{-11}, \\ \frac{\rho_{\text{dm}}}{s} &= \frac{\Omega_{\text{dm}}h^2}{\Omega_b h^2} \frac{m_p n_b}{s} \simeq \frac{0.1194}{0.0221} (938 \text{ MeV})(8.59 \times 10^{-11}) \simeq 0.39 \text{ eV}, \end{aligned} \quad (4.2)$$

thermal QCD results for the entropy density  $s$  and energy density  $\varepsilon$  of the thermal plasma from Borsanyi *et al* [1],

$$\varepsilon(T) = \frac{\pi^2 T^4 g_*}{30}, \quad s(T) = \frac{2\pi^2 T^3 g_*}{45}, \quad g_*(1 \text{ GeV}) \simeq 73, \quad (4.3)$$

$$\chi(T) \simeq \left( \frac{1 \text{ GeV}}{T} \right)^{7.6} (1.02(35) \times 10^{-11} \text{ GeV}^4), \quad (4.4)$$

Hubble's law  $H^2 = 8\pi\varepsilon/(3m_{\text{pl}}^2)$  with  $m_{\text{pl}} \simeq 1.22 \times 10^{19}$  GeV, the thermal value for the axion mass  $m_a^2(T) = \chi(T)/f_a^2$ , and vacuum value  $\chi(T=0) = (0.076 \text{ GeV})^4$  [46], to obtain

$$f_a = (2.21 \pm 0.29) \times 10^{11} \text{ GeV}, \quad (4.5)$$

$$m_a = 26.2 \pm 3.4 \mu\text{eV}, \quad (4.6)$$

$$T_* = 1.54 \pm 0.05 \text{ GeV}. \quad (4.7)$$

Taking the errors quoted in Ref.[1] at face value, the dominant error in  $f_a$  and hence in  $m_a$  is from our determination of  $K$ , while the error in  $T_*$  arises equally from the errors in  $K$  and in  $\chi(T)$ . Eq. (4.5), Eq. (4.6), and Eq. (4.7) constitute the main results of our study.

Our most striking result is that the axion production from random initial conditions, with the resulting dense and high-tension axionic string network, is actually *smaller* than the angle-averaged misalignment value. The deficit gets larger at large  $n$ , where the  $\theta_a$  potential tilts more abruptly; if it tilts more gradually then the axion production exceeds the misalignment value. Furthermore, although axion production is larger from high-tension strings than from strings with a lower tension, the dependence is quite weak; a factor of 10 increase in string tension between our results and the results of [29], along with the resulting factor of 3 increase in the string network density, has led to less than a 30% increase in axion production.

This clearly requires some explanation. The conventional wisdom has been (see for instance [28]) that axions are produced by misalignment in the space between walls, by walls, and by strings. Therefore the production is the sum of three terms, and must be larger than the misalignment contribution. We argue that this picture involves assumptions and commits double counting. It does not make sense to consider misalignment axions to be independent from walls. Within the misalignment mechanism, half of all axions emerge from the range of angles  $|\theta_a(t=0)| \in [2.76, \pi]$ . But it is precisely the regions with  $\theta_a \sim \pi$  which become the domain walls. Much or most of the “misalignment” axion field energy becomes the domain walls; it is double counting to speak of both domain-wall axions and misalignment axions as independent contributions. Of course, since the axion field is initially very inhomogeneous, it is also not obvious that there are *any* spacetime regions where homogeneous misalignment is a useful description.

Consider also what happens to the energy in domain walls. After the potential tilts and the domain walls become relatively thin and distinct, the wall surface tension induces forces on the strings. The walls lose their energy to accelerating the strings, which consumes the wall area (see Figure 3). Also in this epoch, it is not simple for walls or strings to emit axions. The axion frequency  $m_a$  increases with time, and any process involving time scales longer than  $m_a^{-1}$  has a frequency-mismatch problem to produce massive axions. That is, long wavelength fluctuations of walls or strings are incapable of producing axions because they drive the axion field at frequencies below  $m_a$ . We saw this very clearly in our previous study of 2+1D axion production with massive strings [30].

What about the energy of the string network? The high string tension means that the network stores much more energy. But after the time scale  $t_*$ , the energy in domain walls and in axionic fluctuations increases with the axion mass as  $E \propto m_a \propto t^{1+\frac{n}{2}}$ , while the string energy does not increase as  $m_a$  increases. Therefore the string network’s ability to produce axions dilutes with time. The network only annihilates when the walls are able to influence string dynamics, which occurs when the wall energy is comparable to the string energy. That is, the strings only fragment when their energy is comparable to the energy that was present in the wall network which caused them to fragment. And there is still the question of how efficiently the resulting small loops turn their energy into axions.

To improve this analysis, we see a few directions which need to be pursued. First, we

need simulations with more RAM, so that larger boxes, and therefore larger  $mt_*$  values, can be studied. We need to be more systematic in setting the initial network density and understanding the approach to network scaling. It should be straightforward to reduce statistical and extrapolation errors to the few percent level, with the dedication of more computer power.

Also, we would like to investigate some of the late network evolution in more microscopic detail. The string network breaks up into loops which then annihilate in a way which somehow does not produce many axions. It should be possible to cut such loops out of a simulation and resolve them with a much finer lattice, which can then properly separate the  $m_a$  and  $m$  mass scales and follow the loop dynamics down to short scales. This could help explain why so few axions are produced (or determine whether our limited lattice spacing is causing a systematic neglect of some relevant but shorter-distance physics).

## Acknowledgments

We would like to thank Mark Hindmarsh for very useful conversations, and Daniel Robaina, Thomas Jahn, and Max Eller. We also thank the GSI Helmholtzzentrum and the TU Darmstadt and its Institut für Kernphysik for supporting this research.

## A Algorithmic details

Here we explain in more detail how our numerics work. Following Ref. [32], we embed the axion field as a global U(1) symmetry of a theory with two scalars  $\varphi_1, \varphi_2$  and one U(1) gauge symmetry, so one linear combination of the U(1) $\times$ U(1) symmetry is gauged and one is global. Both are spontaneously broken by the scalar vacuum values:

$$\begin{aligned}
 -\mathcal{L}(\varphi_1, \varphi_2, A_\mu) = & \frac{1}{4e^2} F_{\mu\nu} F^{\mu\nu} + \left| (\partial_\mu - iq_1 A_\mu) \varphi_1 \right|^2 + \left| (\partial_\mu - iq_2 A_\mu) \varphi_2 \right|^2 \\
 & + \frac{m_1^2}{8v_1^2} \left( 2\varphi_1^* \varphi_1 - v_1^2 \right)^2 + \frac{m_2^2}{8v_2^2} \left( 2\varphi_2^* \varphi_2 - v_2^2 \right)^2.
 \end{aligned}
 \tag{A.1}$$

Here  $q_1, q_2$  are the field charges with  $q_2 = q_1 - 1$ . The axion is the angle

$$\theta_a = q_2 \text{Arg } \varphi_1 - q_1 \text{Arg } \varphi_2
 \tag{A.2}$$

which is gauge-invariant. This procedure exactly reproduces the global symmetry and the way strings act as a source for the axion field; the dynamics are modified only by a large induced string tension,  $\kappa \simeq 2(q_1^2 + q_2^2)$ , and heavy degrees of freedom which should decouple from the dynamics in the continuum limit (in the sense of  $mt \gg 1$ , or  $mt_* \gg 1$  for our current purposes)[32]. We consider  $v_1 = v_2$  and  $m_1^2 = m_2^2 = e^2(q_1^2 v_1^2 + q_2^2 v_2^2) = m_e^2$  so all heavy fields have a common mass. The axion decay constant is  $f_a^2 = v_1^2 v_2^2 / (v_1^2 q_1^2 + v_2^2 q_2^2)$ . In our lattice units we normalize our fields such that  $v_1 = 1 = v_2$ . The topological susceptibility part of the potential (which breaks the global U(1) symmetry, “tilting” the

potential for the axion field), is implemented as

$$t^2 \chi(t) \left(1 - \cos \text{Arg } \theta_a\right) \Rightarrow \frac{f_a^2 t^{n+2}}{t_*^{n+4}} F(2\varphi_1^* \varphi_1) F(2\varphi_2^* \varphi_2) \left(1 - \cos \left(q_2 \text{Arg } \varphi_1 - q_1 \text{Arg } \varphi_2\right)\right) \quad (\text{A.3})$$

$$F(r) \equiv \begin{cases} \frac{25}{16} r \left(\frac{8}{5} - r\right), & r < \frac{4}{5}, \\ 1, & r > \frac{4}{5}. \end{cases} \quad (\text{A.4})$$

The function  $F(r)$  is inserted to soften the behavior of the susceptibility term in string cores; without this term the introduced potential becomes violently nondifferentiable wherever  $\varphi^* \varphi \sim 0$  for either field, which causes problems for space-discretized equations of motion. The modification only changes the tilted potential inside string cores, where its effect is very subdominant to the leading potential terms. But without this modification we do not get consistently stable evolution near string cores. Our results are insensitive to the specific form of  $F(r)$ , provided  $F(1) = 1$ ,  $F'(1) = 0$ ,  $F(0) = 0$ , and  $F'(r)$  is continuous, which motivated our choice. A similar modification is common in single-scalar simulations of axionic strings, where most authors [19, 28] have made the substitution  $(1 - \cos \text{Arg } \varphi) \rightarrow \sqrt{2} \text{Re } \varphi$ , a substitution which is correct only for the angular dynamics and only where  $2\varphi^* \varphi = 1$ . This replacement is justified because it is simpler, is nonsingular at 0, and is only of much influence outside string cores, where it is nearly equivalent to the correct form. We have explicitly checked that in the single-scalar model, axion production and string dynamics are nearly indistinguishable whether we use  $(1 - \cos \text{Arg } \varphi)$  or  $\sqrt{2} \text{Re } \varphi$  as the “tilt” in the potential.

Our numerical implementation uses a standard leapfrog algorithm and the noncompact formulation of  $U(1)$ . The only novel feature is that we use an  $a^2$ -improved action for both the scalar and gauge parts, which requires a somewhat nontrivial treatment of electric fields in which the link’s canonical momentum is not the same as the link’s time derivative [47]. More details and tests are in [32].

## B Other numerical tests

Here we detail some tests which have little bearing on the extrapolation to a final result, and which we have therefore not put in the main development.

In the main text we spend some effort considering when to stop the growth of  $\chi(T)$ . But we do not discuss when to measure the axion number, arguing only that it is sufficient to measure after the string network is gone and only small fluctuations remain. Here we justify this claim. Figure 7 shows what happens when we measure the axion number before the string network has finished collapsing. The figure shows the density of strings in blue, and the density of axions, as measured at the indicated time, in black. This measurement is somewhat ambiguous because it involves identifying the axion angle  $\theta_a \in [-\pi, \pi]$  which is discontinuous across domain walls. Such a discontinuity leads to “ringing” in the Fourier spectrum and formally gives a logarithmically UV divergent particle number (cut off by lattice effects). We “fix” this problem by truncating the largest  $\theta_a$  values, reflecting  $\theta_a \in$

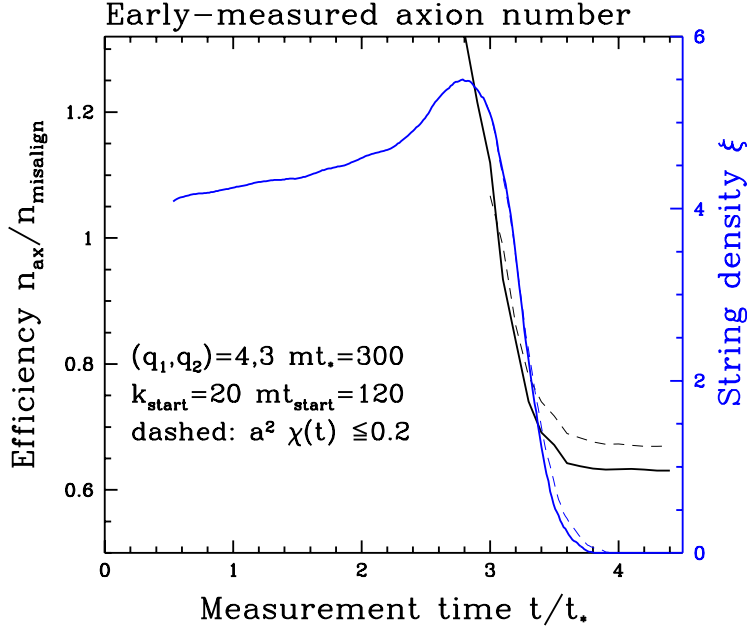


**Figure 7.** Blue: scaled string density  $\xi$  as a function of time. Black: instantaneously measured axion number at the same time. Dashed lines are for an evolution with an upper cutoff on  $\chi(T)$  at  $\chi(T) < m^2/5$ .

$[\pi/2, \pi]$  to  $\theta_a \rightarrow \pi - \theta_a$ , and similarly for  $\theta_a \in [-\pi, -\pi/2]$ . Despite this “cap” on the maximum size of  $|\theta_a| < \pi/2$ , we nevertheless find a very large axion density if we measure axions before the network has decayed. However, we see that after the strings are gone, the axion number becomes completely independent of further time evolution. Our “cap” on large  $\theta_a$  values has no effect on this final plateau, because  $|\theta_a| > \pi/2$  virtually never happens and represents a tiny fraction of the axion number. In light of this result, we generally measure  $n_{\text{ax}}$  as soon as no strings remain, but when we evolve for longer and remeasure later, we get an answer which agrees at the 1% level. If we repeat this analysis for the misalignment scenario, we find that instead of becoming virtually  $t$ -independent at  $t = 4t_*$ , the axion number becomes virtually  $t$ -independent already by  $t = 2t_*$ . This difference reflects the absence of topological structures in the misalignment scenario.

The other test which proves to play almost no role in the final axion density is the box volume. To test out to very large and quite small volumes, we used the rather small value of  $mt_* = 200$ . Keeping everything else besides the volume unchanged, we find in Figure 8 that the volume has less than a  $< 2\%$  effect on the axion abundance down to a box length of  $Lt_* = 2$ . Note that any box larger than  $Lt_* = 8$  should have essentially zero volume dependence, since the box periodicity is invisible for  $Lt > 2$  and the axion number becomes an adiabatic invariant by  $t = 4t_*$ .

The smallest volume shown,  $L = 1.28t_*$ , shows a larger generated axion number, with larger statistical fluctuations (we used more simulations for smaller volumes so the product of simulations and volumes is about the same for each data point). The reason is that, in a small fraction of small- $L$  simulations, after all strings annihilate, there remains a domain

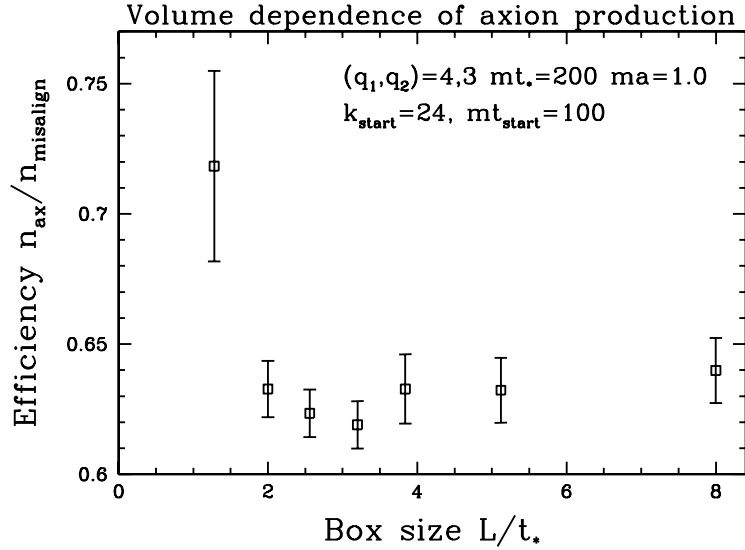


**Figure 8.** Study of box volume dependence of the axion production rate. Except for the smallest volume, it appears the result shows extremely weak volume dependence.

wall stretching across the whole box. This domain wall is metastable and lasts indefinitely, until it dominates the axion number. This is purely a small volume artifact; nothing of the sort ever occurs for the larger volumes.

Because the volume dependence is so mild, it should be possible to study the axion production in boxes down to  $Lt_* = 2$  or 3. However, to be conservative, we have generally tried to keep  $Lt_* \geq 5$ . Recall that there cannot be lattice volume dependence for  $L > 2t$ , and we need  $t = 4t_*$ , so the box size dependence should be exactly zero for  $Lt_* > 8$ . The extremely weak box size sensitivity allows us to relax this value somewhat.

## References

- [1] Sz. Borsanyi et al. Calculation of the axion mass based on high-temperature lattice quantum chromodynamics. *Nature*, 539(7627):69–71, 2016.
- [2] Steven Weinberg. A New Light Boson? *Phys.Rev.Lett.*, 40:223–226, 1978.
- [3] Frank Wilczek. Problem of Strong p and t Invariance in the Presence of Instantons. *Phys.Rev.Lett.*, 40:279–282, 1978.
- [4] Gerard 't Hooft. Computation of the Quantum Effects Due to a Four-Dimensional Pseudoparticle. *Phys.Rev.*, D14:3432–3450, 1976.
- [5] R. Jackiw and C. Rebbi. Vacuum Periodicity in a Yang-Mills Quantum Theory. *Phys. Rev. Lett.*, 37:172–175, 1976.
- [6] Curtis G. Callan, Jr., Roger F. Dashen, and David J. Gross. Instantons as a Bridge Between Weak and Strong Coupling in QCD. *Phys. Rev.*, D20:3279, 1979.
- [7] R.D. Peccei and Helen R. Quinn. CP Conservation in the Presence of Instantons. *Phys.Rev.Lett.*, 38:1440–1443, 1977.

- [8] R.D. Peccei and Helen R. Quinn. Constraints Imposed by CP Conservation in the Presence of Instantons. *Phys.Rev.*, D16:1791–1797, 1977.
- [9] Jihn E. Kim. Weak Interaction Singlet and Strong CP Invariance. *Phys. Rev. Lett.*, 43:103, 1979.
- [10] Mikhail A. Shifman, A. I. Vainshtein, and Valentin I. Zakharov. Can Confinement Ensure Natural CP Invariance of Strong Interactions? *Nucl. Phys.*, B166:493–506, 1980.
- [11] John Preskill, Mark B. Wise, and Frank Wilczek. Cosmology of the Invisible Axion. *Phys. Lett.*, B120:127–132, 1983.
- [12] L. F. Abbott and P. Sikivie. A Cosmological Bound on the Invisible Axion. *Phys. Lett.*, B120:133–136, 1983.
- [13] Michael Dine and Willy Fischler. The Not So Harmless Axion. *Phys. Lett.*, B120:137–141, 1983.
- [14] Luca Visinelli and Paolo Gondolo. Dark Matter Axions Revisited. *Phys. Rev.*, D80:035024, 2009.
- [15] L. Visinelli and P. Gondolo. Axion cold dark matter in view of BICEP2 results. *Phys. Rev. Lett.*, 113:011802, 2014.
- [16] P. A. R. Ade et al. Planck 2015 results. XIII. Cosmological parameters. *Astron. Astrophys.*, 594:A13, 2016.
- [17] Richard Lynn Davis. Cosmic Axions from Cosmic Strings. *Phys. Lett.*, B180:225, 1986.
- [18] M. C. Huang and P. Sikivie. The Structure of Axionic Domain Walls. *Phys. Rev.*, D32:1560, 1985.
- [19] Takashi Hiramatsu, Masahiro Kawasaki, and Ken’ichi Saikawa. Evolution of String-Wall Networks and Axionic Domain Wall Problem. *JCAP*, 1108:030, 2011.
- [20] Takashi Hiramatsu, Masahiro Kawasaki, Ken’ichi Saikawa, and Toyokazu Sekiguchi. Axion cosmology with long-lived domain walls. *JCAP*, 1301:001, 2013.
- [21] Diego Harari and P. Sikivie. On the Evolution of Global Strings in the Early Universe. *Phys. Lett.*, B195:361–365, 1987.
- [22] C. Hagmann, Sanghyeon Chang, and P. Sikivie. Axions from string decay. *Nucl. Phys. Proc. Suppl.*, 72:81–86, 1999.
- [23] R. A. Battye and E. P. S. Shellard. Global string radiation. *Nucl. Phys.*, B423:260–304, 1994.
- [24] R. A. Battye and E. P. S. Shellard. Axion string constraints. *Phys. Rev. Lett.*, 73:2954–2957, 1994. [Erratum: *Phys. Rev. Lett.* 76,2203(1996)].
- [25] Masahide Yamaguchi, M. Kawasaki, and Jun’ichi Yokoyama. Evolution of axionic strings and spectrum of axions radiated from them. *Phys. Rev. Lett.*, 82:4578–4581, 1999.
- [26] Masahide Yamaguchi. Scaling property of the global string in the radiation dominated universe. *Phys. Rev.*, D60:103511, 1999.
- [27] Takashi Hiramatsu, Masahiro Kawasaki, Toyokazu Sekiguchi, Masahide Yamaguchi, and Jun’ichi Yokoyama. Improved estimation of radiated axions from cosmological axionic strings. *Phys.Rev.*, D83:123531, 2011.

- [28] Takashi Hiramatsu, Masahiro Kawasaki, Ken'ichi Saikawa, and Toyokazu Sekiguchi. Production of dark matter axions from collapse of string-wall systems. *Phys.Rev.*, D85:105020, 2012.
- [29] Leesa Fleury and Guy D. Moore. Axion dark matter: strings and their cores. *Journal of Cosmology and Astroparticle Physics*, 2016(01):004, 2016.
- [30] Leesa M. Fleury and Guy D. Moore. Axion String Dynamics I: 2+1D. *JCAP*, 1605(05):005, 2016.
- [31] Olivier Wantz and E. P. S. Shellard. The Topological susceptibility from grand canonical simulations in the interacting instanton liquid model: Chiral phase transition and axion mass. *Nucl. Phys.*, B829:110–160, 2010.
- [32] Vincent B. Klaer and Guy D. Moore. How to simulate global cosmic strings with large string tension. 2017.
- [33] Alexander Vilenkin. Cosmic strings. *Phys. Rev. D*, 24:2082–2089, 1981.
- [34] Neil Turok and Pijushpani Bhattacharjee. Stretching Cosmic Strings. *Phys. Rev.*, D29:1557, 1984.
- [35] David P. Bennett and Francois R. Bouchet. High resolution simulations of cosmic string evolution. *Phys. Rev.*, D41:2408, 1990.
- [36] Evan Berkowitz, Michael I. Buchoff, and Enrico Rinaldi. Lattice QCD input for axion cosmology. *Phys. Rev.*, D92(3):034507, 2015.
- [37] S. Borsanyi, M. Dierigl, Z. Fodor, S. D. Katz, S. W. Mages, D. Nogradi, J. Redondo, A. Ringwald, and K. K. Szabo. Axion cosmology, lattice QCD and the dilute instanton gas. *Phys. Lett.*, B752:175–181, 2016.
- [38] Peter Petreczky, Hans-Peter Schadler, and Sayantan Sharma. The topological susceptibility in finite temperature QCD and axion cosmology. *Phys. Lett.*, B762:498–505, 2016.
- [39] Yusuke Taniguchi, Kazuyuki Kanaya, Hiroshi Suzuki, and Takashi Umeda. Topological susceptibility in finite temperature ( 2+1 )-flavor QCD using gradient flow. *Phys. Rev.*, D95(5):054502, 2017.
- [40] Florian Burger, Ernst-Michael Ilgenfritz, Maria Paola Lombardo, Michael Mller-Preussker, and Anton Trunin. Topology (and axion's properties) from lattice QCD with a dynamical charm. In *26th International Conference on Ultrarelativistic Nucleus-Nucleus Collisions (Quark Matter 2017) Chicago, Illinois, USA, February 6-11, 2017*, 2017.
- [41] J. Frison, R. Kitano, H. Matsufuru, S. Mori, and N. Yamada. Topological susceptibility at high temperature on the lattice. *JHEP*, 09:021, 2016.
- [42] Claudio Bonati, Massimo D'Elia, Marco Mariti, Guido Martinelli, Michele Mesiti, Francesco Negro, Francesco Sanfilippo, and Giovanni Villadoro. Axion phenomenology and  $\theta$ -dependence from  $N_f = 2 + 1$  lattice QCD. *JHEP*, 03:155, 2016.
- [43] Claudio Bonati, Massimo D'Elia, Marco Mariti, Guido Martinelli, Michele Mesiti, Francesco Negro, Francesco Sanfilippo, and Giovanni Villadoro. Recent progress on QCD inputs for axion phenomenology. *EPJ Web Conf.*, 137:08004, 2017.
- [44] Jihn E. Kim. A COMPOSITE INVISIBLE AXION. *Phys. Rev.*, D31:1733, 1985.
- [45] Patrick Fox, Aaron Pierce, and Scott D. Thomas. Probing a QCD string axion with precision cosmological measurements. 2004.

- [46] Giovanni Grilli di Cortona, Edward Hardy, Javier Pardo Vega, and Giovanni Villadoro. The QCD axion, precisely. *JHEP*, 01:034, 2016.
- [47] Guy D. Moore. Improved Hamiltonian for Minkowski Yang-Mills theory. *Nucl. Phys.*, B480:689–728, 1996.